Proceedings of the 9th World Congress on Mechanical, Chemical, and Material Engineering (MCM'23)
Brunel University, London, United Kingdom –August 06-08, 2023
Paper No. HTFF 161
DOI: 10.11159/htff23.161

A Novel Battery Thermal Management System based on Capillary Driven Evaporative Cooling

Delika M. Weragoda[1], Guohong Tian[1], Qiong Cai[2]
[1]School of Mechanical Engineering Sciences, Faculty of Engineering and Physical Sciences, University of Surrey, Guildford GU2 7XH, UK
d.weragoda@surrey.ac.uk; g.tian@surrey.ac.uk
[2]Department of Chemical and Process Engineering, Faculty of Engineering and Physical Sciences, University of Surrey, Guildford GU2 7XH, UK
q.cai@surrey.ac.uk

Abstract **–** In this paper we present an experimental and a numerical study on a novel battery thermal management system (BTMS) based on capillary driven evaporative cooling (CDEC). The experimental study was conducted using Cu foam and Novec 7000 to determine the cooling performance of this system when cooled through a single surface of the battery at three different heating inputs: 10W, 20W and 30W. The system was further expanded to incorporate cooling from the two larger surfaces of the battery using a numerical model. Results from the experimental study showed that the maximum temperature of battery can be maintained below 50℃ for a heat input of 30W, when the cell is cooled using a single surface. This was further reduced to 40℃ when cooled from both surfaces. Furthermore, these temperatures were achieved through partial wetting of the battery surface due to a capillary rise of about 11% of the total battery height. This clearly demonstrates the superior cooling capabilities of this novel BTMS. However, the maximum temperature different recorded in the battery at a heat input of 30W was 5.47℃ which was a result of the uneven cooling rates in the wetted and non-wetted regions of the battery due to partial capillary rise.

Keywords**:** Capillary driven evaporative cooling, battery cooling, Novec 7000, wick structure

1. Introduction

The necessity to match the performance of electric vehicles (EV) with conventional gasoline and diesel vehicles, has resulted in an increasing interest in the demand for high energy dense, fast chargeable, and dischargeable Lithium ion (Li-ion) batterie. Li-ion batteries operate on the principle of intercalation, deintercalation and charge transfer via the electrolyte [1], [2] generate heat (both reversible and irreversible) [3], [4] that would considerably increase the internal temperature of the battery leading to catastrophic events such as thermal runaway, if not properly maintained by thermal management [5]. Therefore, thermal management of Li-ion batteries has become more important than ever. Battery thermal management (BTM) serves the purpose of maintaining the maximum temperature of Li-ion batteries within the optimum limits of 15℃ - 35℃ [6], [7] and the temperature uniformity within 5℃, to avoid loss of capacity and even thermal runaway.

Recent reviews by Weragoda et al. [8], Roe et al.[9], Zhao et al. [10] and Bernagozzi et al. [11] have shown that passive cooling techniques such as heat pipe (HP) based BTM, phase change material (PCM) based BTMS, and immersion cooling have gained the attention of the research community in utilizing for thermal management of EV batteries. These passive cooling methods have shown promising results in maintaining the battery temperature within its operating limits. However, the authors have identified several issues that have to be addressed if these techniques are to be commercialized. One of the key issues identified in HPBTM is their comparatively small thermal contact area between heat pipes and the battery. To improve this thermal contact area, heat pipes have to either be combined with PCM, thermal grease, or high thermal conductive metal plates, that would add another layer of thermal resistance and weight to the thermal management system [8]. Similarly, the addition weight when using complete immersion cooling and PCM also hinders the packs overall energy density [9], [10].

Therefore, to address these issues of added weight and thermal resistance, we propose a novel battery thermal management based on capillary driven evaporative cooling (CDEC). This paper outlines the theory behind this mechanism and a numerical approach investigating the cooling effectiveness of CDEC in a partially wetted battery. The numerical model

is validated using experimental data and the results are presented in terms of temperature profiles to highlight the effectiveness of cooling using CDEC method.

2. Methodology

2.1. Capillary driven evaporative cooling cycle.

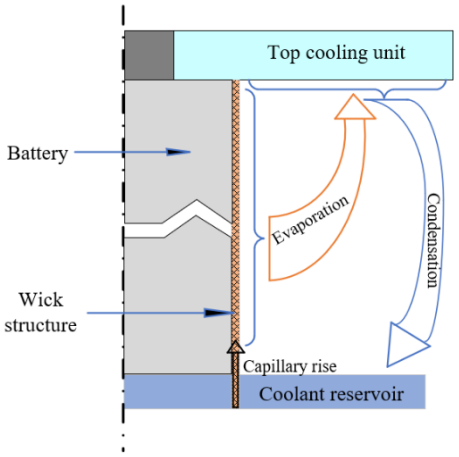

Fig. 1: Schematic diagram of the CDEC system

Figure 1 represents a schematic diagram of the cycle representing CDEC, where a wick structure made of high thermal conductive material is directly attached to the surface of the battery. This wick structure provides the required capillary pressure to raise the working fluid (coolant) through the structure wetting the surface of the battery. The heat generated by the battery during charging and discharging will be absorbed by the working fluid, raising the temperature of the liquid while cooling the battery. When the temperature of the working fluid reaches its saturation temperature the fluid changes its phase absorbing latent heat. The saturation temperature will either be controlled by the operating pressure of the CDEC system or by means of utilizing working fluid with low saturation temperature such as Novec 7000. Once the working fluid changes its phase the vapourised working fluid will be driven by buoyancy towards the top cooling unit, where it will condense and be directed back to the coolant reservoir at the bottom of the chamber completing one cycle of the CDEC process.

2.2. Experimental setup

Figure 2 shows the experimental setup consisting of a closed chamber made of acrylic that is used to maintain the operating conditions of the system. Two heater cartridges are inserted into an aluminium (Al) metal block ($90mm \times 70mm \times 27mm$) to replicate the battery. A copper (Cu) foam is attached to one of the surfaces of the Al metal block while all other surfaces of the Al block are insulated using insulating tape. The Al block (battery) is placed in such a way that it is above the pool of working fluid, while 10mm of the Cu foam is below this pool assuring there is sufficient working fluid to saturate the wick structure during operation. The cooling unit is equipped with two internal heat sinks, two Peltier elements, an external heat sink and a fan to maintain the chamber temperature around 20℃. The temperature measuring points (T_1 – T_4) are used to monitor the variation of temperature along the surface of the battery. K-type thermocouples with an uncertainty of ± 0.5℃ are connected to a data acquisition unit (DAQ) to record the temperature variation of the battery at different heat inputs.

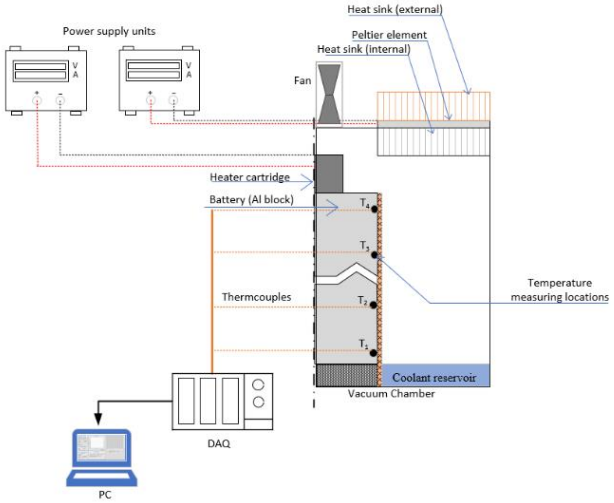

Fig. 2: Experimental setup

2.3. Numerical modelling

A numerical model is developed to analyse the performance of the CDEC system. For this a thermal resistance network model as shown in Figure 3 is develop using MATLAB Simscape, incorporating the conductive, convective, evaporative heat transfers and the thermal masses of both the wetted and non-wetted regions of the battery and the wick. The model incorporates a function block defined using Eqs. (3) and (10) that monitors the surface temperature of the battery and switches from convective heat transfer to evaporative heat transfer in the wetted region.

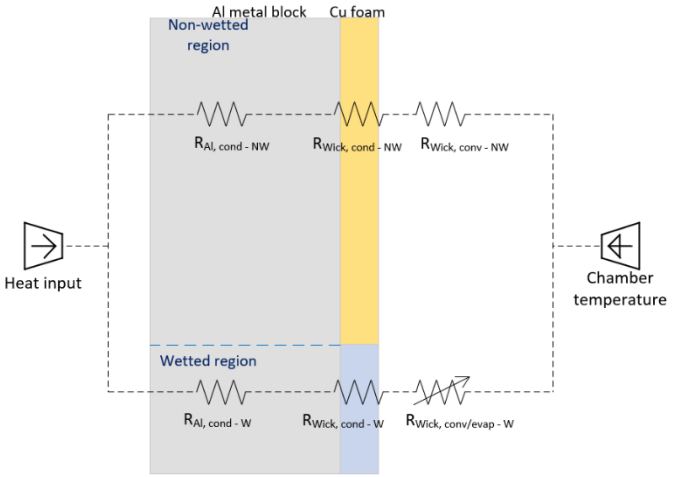

Fig. 3: Thermal resistance network model for the CDEC system

The wick structure used in this experiment is a Cu foam of pore density and porosity of 130PPI and 0.76, respectively. The effective thermal conductivity of the wick structure in both the wetted and non-wetted regions are defined using Eqs. (1) proposed by Bhattacharya et al. [12].

$$k_e = A\left(\varepsilon k_f + (1-\varepsilon)k_s\right) + \frac{1-A}{\left(\frac{\varepsilon}{k_f}+\frac{1-\varepsilon}{k_s}\right)} \quad (1)$$

where, A is a fitting parameter based on experimental data, ε is the porosity of the sample, k_f is the thermal conductivity of the fluid phase and k_s is the thermal conductivity of the solid phase. The Weiner and the Maxwell equations also known as Hashim-Shtrikman bounds have been extensively used to develop several other models to determine the effective thermal conductivity of multiphase structures [13], [14]. Such derived effective thermal conductivity models and models that characterize the heat transfer through different types of wick structures such as metallic foams and screen mesh are highlighted in ref. [15]–[21].

The heat conducted through the wick structure is transferred to the atmosphere adjacent to the wick surface through convective heat transfer. Bhattacharya et al. [22] in their work on buoyancy-induced convection describes how the heat from metallic foams is dissipated to the surrounding based on different orientation of the foams. For a vertically oriented metallic foam, the correlation given in Eqs. (3) was suggested.

$$Nu = 38.94 Ra_L^{0.25} Da^{0.23} \tag{2}$$

Here, the Nusselt number (Nu), Rayleigh number (Ra) and the Darcy number (Da) at a particular vertical length (L) were defined in terms of the permeability of the wick structure and were given by Eqs. (3) - (5) respectively.

$$Nu = \frac{hL}{k_e} \tag{3}$$

$$Da = \frac{K}{L^2} \tag{4}$$

$$Ra_L = \frac{g\beta(T_b - T_{amb})KL}{\alpha_e v_f} \tag{5}$$

where, K is the permeability, L represents the length or height (vertical) of the metal foam, g is the acceleration due to gravity, α_e is the effective thermal diffusivity, β the coefficient of thermal expansion of the fluid, v_f is the kinematic viscosity of fluid, T_b is the battery temperature (or block temperature) and T_{amb} is the ambient temperature to which the metal foam is exposed to. Eqs. (6), defined in terms of the tortuosity τ and the hydraulic diameter d can be used to determine the permeability of the metallic foam structure [23].

$$\frac{K}{d^2} = \frac{\varepsilon^2}{36\tau(\tau - 1)} \tag{6}$$

The hydraulic diameter (d) and the tortuosity (τ) parameters can be estimated using Eqs. (7) – (8) respectively [12].

$$d = d_p \sqrt{\frac{\tau}{3\varepsilon}} \tag{7}$$

$$\frac{1}{\tau} = \frac{\pi}{4\varepsilon} \left\{ 1 - \left(1.18 \sqrt{\frac{(1-\varepsilon)}{3\pi}} \frac{1}{G} \right)^2 \right\} \tag{8}$$

where, G is a geometric function that characterizes the structure of the metallic foam. The effective thermal diffusivity defined by the ratio of effective thermal conductivity (k_e) and the product of effective density (ρ_e) and effective specific heat capacity (C_{pe}) is given by Eqs. (9).

$$\alpha_e = \frac{k_e}{\rho_e C_{pe}} = \frac{k_e}{[\varepsilon\rho_f + (1-\varepsilon)\rho_s][\varepsilon C_{pf} + (1-\varepsilon)C_{ps}]} \tag{9}$$

where $\rho_f, \rho_s, C_{ps}, C_{pf}$ represent the density and specific heat capacity at constant pressure of the constituent working fluid and the solid structure.

The effective heat transfer coefficient for evaporation of liquid to vapour can be determined using Eqs. (10) obtained from kinetic theory [15].

$$h_{lv} = \frac{2\sigma}{2-\sigma}\frac{h_{fg}^2}{T_{sat}v_{fg}}\left(\frac{1}{2\pi RT_{sat}}\right)^{\frac{1}{2}}\left(1 - \frac{P_{sat}v_{fg}}{2h_{fg}}\right) \quad (10)$$

where, $v_{fg,}$ T_{sat}, P_{sat}, R and h_{fg} represent the specific volume change, saturation temperature, saturation pressure, gas constant and the latent heat of vapourization of the working fluid respectively. The accommodation coefficient (σ) depends on both the structure and the working fluid and characterizes the efficiency of energy transfer at the liquid-vapour interface. Here, in this study the correlation for evaporative heat transfer coefficient is used to determine the heat transfer from the surface of the wetted region of the CDEC system assuming that the adjacent region is saturated with the vapour of the constituent working fluid. The heat transfer due to evaporation (Q_{evap}) across the wetted region can be expressed by Eqs. (11), by considering the porosity and the area of the wetted region.

$$Q_{evap} = h_{lv}\varepsilon A_w \Delta T \quad (11)$$

The heat transfer across the wick structure can be evaluated using Eqs. (12) – (14), where the Fourier's law of conduction and Newton's law of cooling given by Eqs. (12) – (14) can be used to describe the conductive heat transfer (Q_{cond}), convective heat transfer (Q_{conv}) and the heat capacity (Q) respectively of the constituent components of the CDEC system.

$$Q_{cond} = kA_{total}\nabla T \quad (12)$$
$$Q_{conv} = hA_{total}\Delta T \quad (13)$$
$$Q = mC\Delta T \quad (14)$$

3. Results and discussion

Figure 4a shows the temperature variation of the points T_1-T_4 of the battery at three different heat inputs 10W, 20W and 30W. It can be clearly seen that the CDEC system incorporating Novec 7000 as the working fluid is capable of maintaining the maximum temperature of the cell below 50℃ at a heat input of 30W, even when the battery is cooled from a single surface with a wetted area of 11%. However, the maximum temperature different of the battery at this condition was recorded to be slightly above the recommended range of 5℃ as seen from Figure 4b. This difference in temperature distribution of the battery surface for this experiment is associated with the uneven cooling in the wetted and the non-wetted regions. The cooling in the wetted region is dominated by convective and evaporative heat transfer of the working fluid, whilst the cooling in the non-wetted region is driven by buoyancy flows of the air/vapour mixture. The effects of heat transfer due to thermal conductivity of the wick structure in the two region does not have a considerable difference since the effective thermal conductivity of the wick structure is dominated by the thermal conductivity of the solid phase (Cu), as the ratio of thermal conductivity of solid phase [8] to liquid phase [24] (k_s/k_l) is in the order of 1000s. On the other hand, Figure 4c shows how the rate of change of temperature in the two regions (wetted and non-wetted) vary at different heat inputs. It can be clearly seen that the rate of change of temperature reaches a quasi-steady state after about 800s. This variation is distinctly seen for the two cases of 20W and 30W, as the temperature of the battery reaches the saturation temperature of the working fluid of 34℃. However, since only about 11% of the battery is wetted by Novec 7000, this quasi-steady state is reached at a slightly higher temperature when a heat input of 30W is supplied. Nonetheless, the effect of phase change is reflected in both 20W and 30W.

To determine the cooling effectiveness of the CDEC system when the battery is cooled from both the large surfaces of the battery ($90mm \times 70mm$), a simple model was developed. The fitting parameters (A, G, and sigma) of the model were determined by initially modelling a single surface cooling model and parameterising against the experimental data.

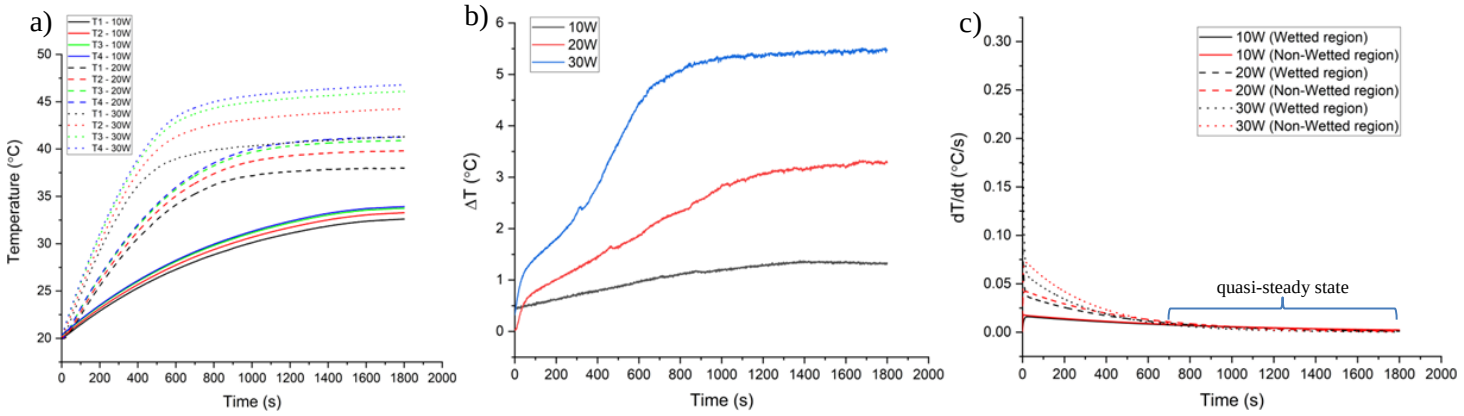

Fig. 4: a) Temperature variation of the battery at the four monitoring points, b) Maximum temperature different recorded c) the rate of change of temperature in the wetted and non-wetted regions at 10W, 20W and 30W.

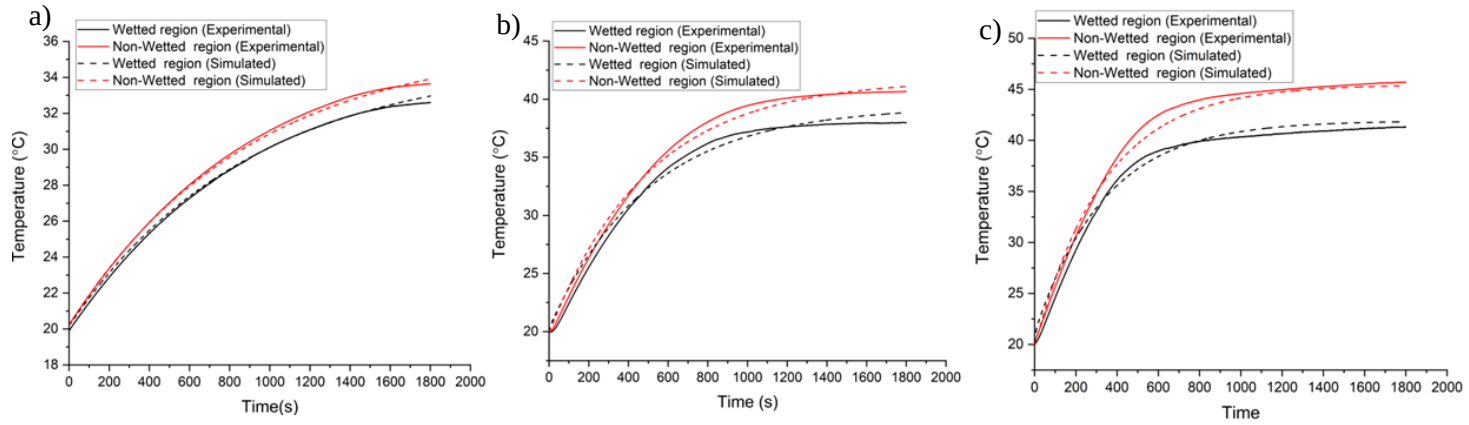

Fig. 5: Simulated vs Experimental temperature profiles for a single ended cooling of the battery using Novec 7000 at a) 10W, b) 20W and c) 30W after parameterizing the model.

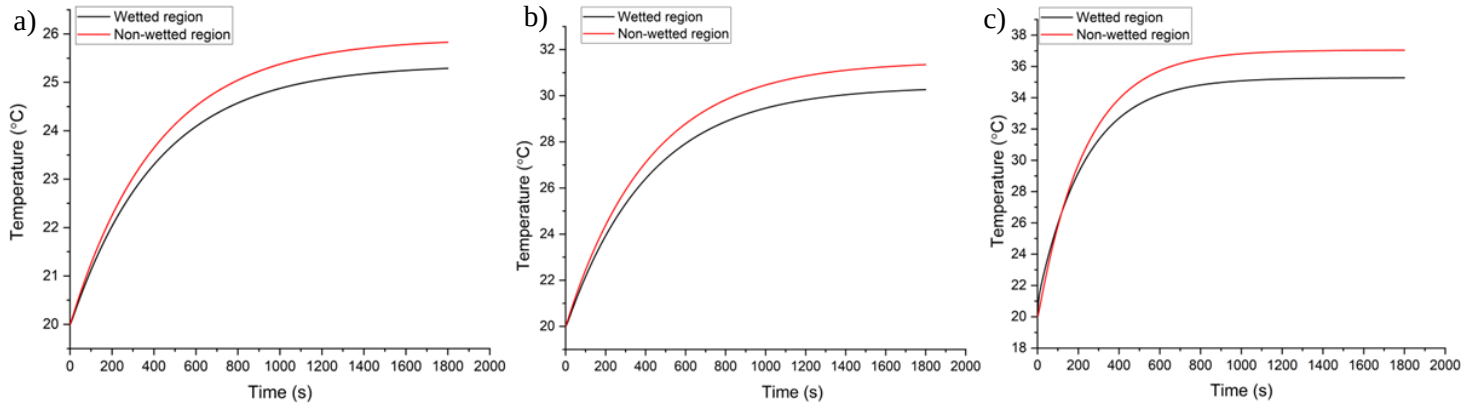

Fig. 6: Simulated temperature profiles for two-sided cooling of the battery using Novec 7000 at a) 10W, b) 20W and c) 30W.

The simulated temperature profiles alongside the experimental data at 10W, 20W and 30W after the parameter estimation process is shown in Figures 5a – c. These parameters were then used in the expanded model where both

90mm x 70mm surfaces of the battery were cooled. It is assumed that both surfaces have cooling rates and wetting areas similar to that of a single surface cooled battery. It can be clearly seen from Figures 6a – c that when the battery is cooled from both surfaces, the average temperature of the wetted and the non-wetted region can be further reduced to below 40°C, 40°C, even at a heat input of 30W. This clearly demonstrates the effectiveness of cooling when utilizing this novel concept concept of CDEC.

It should however be noted that this system can be further improved by incoporating a wick structure with higher pumping pressures either by using a sintered wick structure with comparatively smaller pores and/or improving the hydrophilicity of the strucuture. The main advantage in utilizing Novec 7000 as the working fluid in this system is its low boiling point of 34°C at an ambience of 1 bar. However, if other working fluids are to be used, the operating pressure will have to be controlled to induce saturation around the optimum operating temperature of the battery [25]. The main disadvantage of using Novec 7000 is it relatively high density and low surface tension property, which hinder the capillary pumping forces due to effects of gravity. Therefore further research is required to determine appropriate compability working fluid and methods of improving the hydrophilicity of the wick structure to assure sufficient capillary rise and saturation of the wick structure.

4. Conclusion

In the paper, the performance of a novel battery thermal management system based on capillary driven evaporative cooling is investigated using the temperature variation at three different heat inputs. A simple thermal resistance network model is used to expand the experimental results of a single surface cooling to two-surface cooling to determine the cooling effectiveness of the system. It was shown that with single surface cooling the maximum temperature of the battery can be kept below 50°C when a continuous heat of 30W is supplied for a duration of 30 minutes. This temperature can further be reduced to below 40°C when cooled from the two larger surfaces of the battery. However, it was found that the maximum temperature difference of the battery was slightly higher than the recommended value of 5°C. Further studies will be performed to improve the temperature distribution of the battery by effectively saturating the entire with structure. This could be achieved by reducing the pore size and enhancing the hydrophilicity of the wick structure.

Acknowledgements

Participation in the conference was financially supported by the School of Mechanical Engineering Science, University of Surrey.

References

[1] A. Tomaszewska, Z. Chu, X. Feng, S. O'Kane, X. Liu, J. Chen, C. Ji, E. Endler, R. Li, L. Liu, Y. Li, S. Zheng, S.Vetterlein, M. Gao, J. Du, M.Parkes, M. Ouyang, M. Marinescu, G. Offer, and B. Wu "Lithium-ion battery fast charging: A review," *eTransportation*, vol. 1, p. 100011, Aug. 2019, doi: 10.1016/j.etran.2019.100011.

[2] D. Bernardi, E. Pawlikowski, and J. Newman, "A General Energy Balance for Battery Systems," *J. Electrochem. Soc.*, 1985.

[3] S. Santhanagopalan, K. Smith, J. Neubauer, G.-H. Kim, M. Keyser, and A. Pesaran, *Design and Analysis of Large Lithium-Ion Battery Systems*. Boston: Artech House, 2015.

[4] X. Zhang, "Thermal analysis of a cylindrical lithium-ion battery," *Electrochim. Acta*, vol. 56, no. 3, pp. 1246–1255, Jan. 2011, doi: 10.1016/j.electacta.2010.10.054.

[5] A. W. Golubkov, R. Planteu, P. Krohn, B. Rasch, B. Brunnsteiner, A. Thaler and V. Hacker "Thermal runaway of large automotive Li-ion batteries," *RSC Adv.*, vol. 8, no. 70, pp. 40172–40186, 2018, doi: 10.1039/c8ra06458j.

[6] A. A. Pesaran, "Battery thermal models for hybrid vehicle simulations," *J. Power Sources*, vol. 110, no. 1, pp. 377–382, 2002, doi: 10.1016/s0378-7753(02)00200-8.

[7] Q. Wang, B. Jiang, B. Li, and Y. Yan, "A critical review of thermal management models and solutions of lithium-ion batteries for the development of pure electric vehicles," *Renew. Sustain. Energy Rev.*, vol. 64, pp. 106–128, Oct. 2016, doi: 10.1016/j.rser.2016.05.033.

[8] D. M. Weragoda, G. Tian, A. Burkitbayev, K.-H. Lo, and T. Zhang, “A comprehensive review on heat pipe based battery thermal management systems,” *Appl. Therm. Eng.*, vol. 224, p. 120070, Apr. 2023, doi: 10.1016/j.applthermaleng.2023.120070.

[9] C. Roe *et al.*, “Immersion cooling for lithium-ion batteries – A review,” *J. Power Sources*, vol. 525, p. 231094, Mar. 2022, doi: 10.1016/j.jpowsour.2022.231094.

[10] Y. Zhao, B. Zou, T. Zhang, Z. Jiang, J. Ding, and Y. Ding, “A comprehensive review of composite phase change material based thermal management system for lithium-ion batteries,” *Renew. Sustain. Energy Rev.*, vol. 167, p. 112667, Oct. 2022, doi: 10.1016/J.RSER.2022.112667.

[11] M. Bernagozzi, A. Georgoulas, N. Miché, and M. Marengo, “Heat pipes in battery thermal management systems for electric vehicles: A critical review,” *Appl. Therm. Eng.*, vol. 219, p. 119495, Jan. 2023, doi: 10.1016/j.applthermaleng.2022.119495.

[12] A. Bhattacharya, V. V. Calmidi, and R. L. Mahajan, “Thermophysical properties of high porosity metal foams,” *Int. J. Heat Mass Transf.*, vol. 45, no. 5, pp. 1017–1031, Feb. 2002, doi: 10.1016/S0017-9310(01)00220-4.

[13] F. Tong, L. Jing, and R. W. Zimmerman, “An effective thermal conductivity model of geological porous media for coupled thermo-hydro-mechanical systems with multiphase flow,” *Int. J. Rock Mech. Min. Sci.*, vol. 46, no. 8, pp. 1358–1369, Dec. 2009, doi: 10.1016/j.ijrmms.2009.04.010.

[14] Z. Hashin and S. Shtrikman, “A Variational Approach to the Theory of the Effective Magnetic Permeability of Multiphase Materials,” *J. Appl. Phys.*, vol. 33, no. 10, p. 3125, Jun. 2004, doi: 10.1063/1.1728579.

[15] S. Sudhakar, J. A. Weibel, and S. V. Garimella, “A semi-empirical model for thermal resistance and dryout during boiling in thin porous evaporators fed by capillary action,” *Int. J. Heat Mass Transf.*, vol. 181, 2021, doi: 10.1016/j.ijheatmasstransfer.2021.121887.

[16] Y. Yao, H. Wu, and Z. Liu, “A new prediction model for the effective thermal conductivity of high porosity open-cell metal foams,” *Int. J. Therm. Sci.*, vol. 97, pp. 56–67, Nov. 2015, doi: 10.1016/J.IJTHERMALSCI.2015.06.008.

[17] J. Wang, J. K. Carson, M. F. North, and D. J. Cleland, “A new structural model of effective thermal conductivity for heterogeneous materials with co-continuous phases,” *Int. J. Heat Mass Transf.*, vol. 51, no. 9–10, pp. 2389–2397, May 2008, doi: 10.1016/j.ijheatmasstransfer.2007.08.028.

[18] J. Wang, J. K. Carson, M. F. North, and D. J. Cleland, “A new approach to modelling the effective thermal conductivity of heterogeneous materials,” *Int. J. Heat Mass Transf.*, vol. 49, no. 17–18, pp. 3075–3083, Aug. 2006, doi: 10.1016/j.ijheatmasstransfer.2006.02.007.

[19] Y. Shen, P. Xu, S. Qiu, B. Rao, and B. Yu, “A generalized thermal conductivity model for unsaturated porous media with fractal geometry,” *Int. J. Heat Mass Transf.*, vol. 152, p. 119540, May 2020, doi: 10.1016/j.ijheatmasstransfer.2020.119540.

[20] J. Velardo, A. Date, R. Singh, J. Nihill, A. Date, and T. L. Phan, “On the effective thermal conductivity of the vapour region in vapour chamber heat spreaders,” *Int. J. Heat Mass Transf.*, vol. 145, p. 118797, Dec. 2019, doi: 10.1016/j.ijheatmasstransfer.2019.118797.

[21] V. V. Calmidi and R. L. Mahajan, “The Effective Thermal Conductivity of High Porosity Fibrous Metal Foams,” *J. Heat Transfer*, vol. 121, no. 2, pp. 466–471, May 1999, doi: 10.1115/1.2826001.

[22] A. Bhattacharya and R. L. Mahajan, “Metal foam and finned metal foam heat sinks for electronics cooling in buoyancy-induced convection,” *J. Electron. Packag. Trans. ASME*, vol. 128, no. 3, pp. 259–266, 2006, doi: 10.1115/1.2229225.

[23] P. Du Plessis, A. Montillet, J. Comiti, and J. Legrand, “Pressure drop prediction for flow through high porosity metallic foams,” *Chem. Eng. Sci.*, vol. 49, no. 21, pp. 3545–3553, 1994, doi: 10.1016/0009-2509(94)00170-7.

[24] “3M, 3MTM NovecTM 7000 Engineering Fluid,” 2021. https://multimedia.3m.com/mws/media/121372O/3m-novec-7000-engineered-fluid-tds.pdf (accessed Sep. 15, 2022).

[25] S. Ma, M. Jianga, P. Tao, C. Song, J. Wu, J. Wang, T. Deng, and W. Shang “Temperature effect and thermal impact in lithium-ion batteries: A review,” *Prog. Nat. Sci. Mater. Int.*, vol. 28, no. 6, pp. 653–666, 2018, doi: 10.1016/j.pnsc.2018.11.002.